Heliyon 9 (2023) e13358

Contents lists available at ScienceDirect

Heliyon

journal homepage: www.cell.com/heliyon

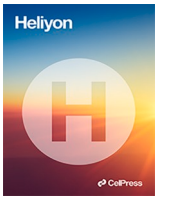

Research article

High sensitivity temperature sensor based on polymer-liquid modified anti-resonant reflecting guidance in silica capillary

Wei Cheng, Shuhui Liu *, Panting Niu, Ting Chen

Hubei Key Laboratory of Optical Information and Pattern Recognition, Wuhan Institute of Technology, Wuhan 430205, China

ARTICLE INFO

Keywords:
Anti-resonant reflecting guidance
UV-Curable adhesive
Temperature sensor

ABSTRACT

A high sensitivity temperature sensor based on polymer and liquid modified anti-resonant reflection principle is proposed. The sensor is made of a section of liquid-filled and UV-curable adhesive coated silica capillary, sandwiched between single mode fibers. The guiding mechanism of the waveguide is affected by both the liquid inside the hollow core, and the adhesive outside the silica cladding. The location of the resonant dips are influenced by the refractive index (RI) of the liquid, while the fringe visibility (resonant strength) is tuned by the both the liquid and the adhesive. By carefully selecting the refractive index value of the infiltrated liquid, and controlling the curing time of the adhesive, sharp resonant dips can be obtained. The sensor exhibits very high temperature sensitivity against temperature. A high sensitivity of 3.369 nm/°C is achieved with an infiltration index of 1.39, in the temperature range from 25 °C to 60 °C. The detection limit of the proposed sensors are 0.04 °C. Moreover, the temperature sensitivity of the sensor is found to be decreasing with the order of resonance. The sensor is easy to fabricate and cost effective, and is applicable in both dry and wet environments, which can find wide applications in biochemical and pharmaceutical industry.

1. Introduction

Fiber-optic temperature sensors offer unique advantages, such as immunity to electromagnetic interferences, repeatability, high stability, high resolution, and fast response. Measurement of temperature using fiber optics has been extensively investigated using various techniques, such as fiber gratings and fiber interferometers. Fiber Bragg gratings (FBG) [1–3] have attracted much attention due to wavelength multiplexing features, but they suffer from relatively low temperature sensitivities (~0.01 nm/°C). Long-period fiber gratings (LPFG), which exhibit higher sensitivity (~0.1 nm/°C) as a temperature sensor, however have undesirable changes in the spectral response due to the high bending sensitivity [4]. Other temperature sensors based on fiber interferometers, such as thin polarization maintaining fiber (PMF) based Sagnac loop [5–7], have relatively lower sensitivities. Photonic Crystal fibers generally have periodic air holes running through the entire fiber length, in which various materials can be filled to achieve different sensing functions [8–14]. Introducing material into fiber structures is an effective method to improve the temperature sensitivity of optical fiber sensors [15–23]. By utilizing the high thermo-optic coefficient of the materials, the temperature sensitivity of these sensors usually increases over an order of magnitude compared with those sensors without the materials using the same sensing principle [24]. For example, by infiltrating a solid core photonic crystal fiber (PCF) with liquids of the high index value, bandgap-like effect is introduced to the fiber, so that very high temperature sensitivity is achieved [25]. By selectively filled the cladding hole of a simplified

* Corresponding author.
E-mail address: liushuhui@wit.edu.cn (S. Liu).

https://doi.org/10.1016/j.heliyon.2023.e13358
Received 21 November 2022; Received in revised form 19 January 2023; Accepted 29 January 2023
Available online 1 February 2023

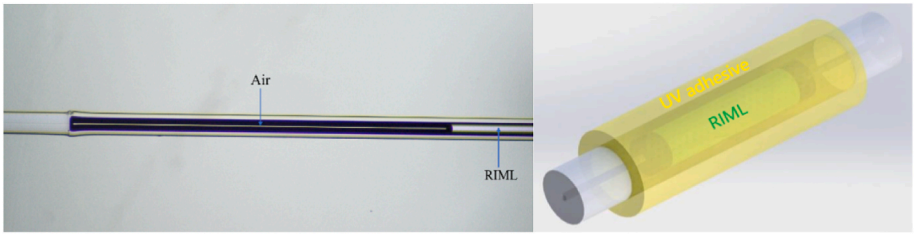

Fig. 1. (a) Photograph of the splicing joint of single mode fiber and the capillary. (b) The schematic structure of the proposed sensor.

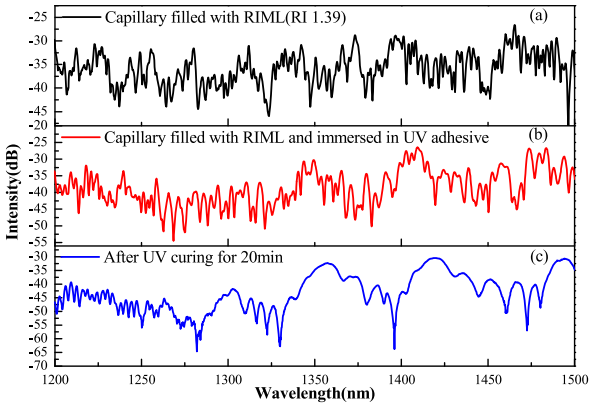

Fig. 2. Transmission spectra of (a): Capillary filled with RIML(RI 1.39). (b): Capillary filled with RIML and immersed in UV adhesive. (c): After UV curing for 20 min.

hollow core PCF with alcohol to modify the anti-resonant reflecting guidance of the fiber, and a temperature sensitivity of −0.46 nm/°C is obtained [26]. However, infiltrating liquids into a specific air hole of a PCF usually requires complicated process like femtosecond laser assisted drilling to selectively open the target air hole, which increases the cost of the sensors.

In our previous work, the transmission mechanism of a silica capillary is altered by introducing liquid inside and outside the silica capillary, and high sensing performance is achieved [27]. However, liquid environment is required for the operation of the sensor, which restricts its application in dry fields. In this work, we presents a highly sensitive temperature sensor based on a modified fiber structure. The sensor consists of a section of silica capillary spliced between single mode fibers. The capillary is filled with refractive index matching liquids (RIML), and is also coated with UV-curable adhesive. The RIML together with the adhesive modifies the anti-resonant reflecting guiding property of the silica capillary by changing the resonant wavelength and resonant strength. Experimental results show that the transmission spectrum of the sensor exhibits redshift response when the ambient temperature rises, and a sensitivity of 3.369 nm/°C is achieved with a device filled with the liquid index value of 1.39, in the temperature range of 25 °C–60 °C. The influence of the index value of the infiltrate liquids on the sensitivity is also investigated. The proposed temperature sensor features a simple fabrication process, low cost and high sensitivity, which can find wide applications in the biochemical and pharmaceutical industry, where high precision temperature measurement is needed.

2. Fabrication and principle of the fiber sensor

The silica capillary (Polymicron Ltd) we used to construct the sensor has an outer diameter of 125 μm, and a hollow core diameter of 75 μm. To infiltrate the silica tube with refractive index matching liquid, one end of the silica tube is immersed in the liquid. Due to the capillary effect, the liquid quickly fills the silica capillary. A liquid with a refractive index of 1.39 was chosen from a series of RIML developed by Cargille Lab for the fabrication of the sensor. The index value of the chosen liquid is close to that of the cured UV adhesive, which could help to improve the spectrum quality of the device. After the infiltration, the liquid-filled capillary is spliced to single mode fibers at both ends with a fusion splicer (Fujikura 80s), the splicing parameter of which is optimized to minimize the deformation of the hollow core at the splicing joints. It can also be seen from Fig. 1(a) that there is a small amount of liquid evaporation at the arc discharge splice. Then the capillary is dipped in a UV-curable adhesive (NOA13685, Norland Products, Inc) and then exposed to UV light for 20 min to make sure that the sharp resonant dips can be obtained. The refractive index (RI) of the adhesive is 1.3685 before cured, and the energy density required for full curing is 6 J/cm2. Fig. 1(b) illustrates the schematic structure of the proposed sensor. The transmission spectrum of the sensor is collected by a broadband source and an optical spectrum analyzer (Yokogawa 6370C).

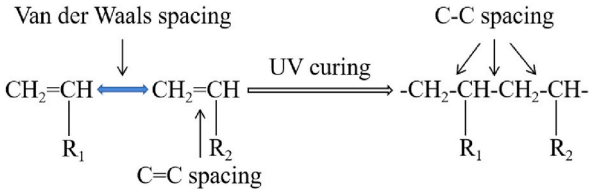

Fig. 3. The Change of atom chemical bonds during the curing process of UV adhesive.

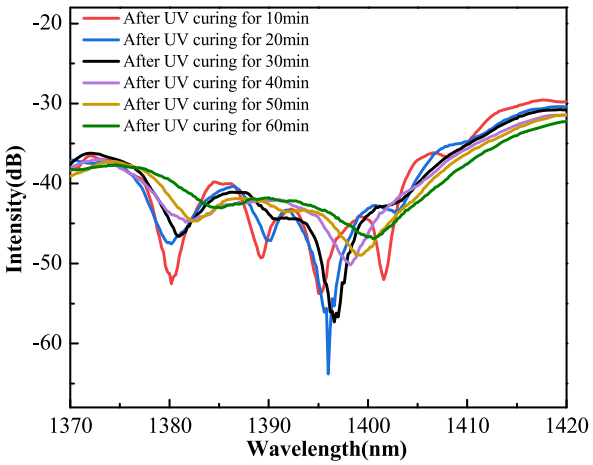

Fig. 4. The change of transmission spectrum of capillary filled with RIML(RI 1.39) and immersed in UV glue with increasing curing time.

For an empty silica capillary (not infiltrated or coated), the guiding principle of the waveguide is based on the anti-resonant reflecting mechanism. The ring cladding of the silica capillary is considered as an F–P etalon, and waves that satisfy the resonant condition of the etalon will leak out of the cladding, while those that do not satisfy the resonant condition can be guided through the hollow core [28]. However, when RIML (RI = 1.39) is filled into the hollow core of the silica capillary, the resonant condition of the etalon is altered, leading to the change of the resonant wavelength, as well as the resonant strength. The anti-resonant reflecting fringe is not much obvious compared with that of the empty capillary. This is because the reflection coefficient at the liquid-silica interface is much smaller compared to the air-silica interface, which weakens the strength of the resonance. The light intensity at resonant wavelength can be expressed as [29]:

$$T_{resonant} = \frac{(1 - rr')^2}{1 + r'^4 - 2r'^2} I_{\text{resonant}} \tag{1}$$

where r and r' respectively represent the reflection coefficients of the inner and outer surfaces of capillary cladding, and I_{resonant} is the input light intensity. Eq. (1) shows when r has a close absolute value as r', the value of T_{resonant} is relatively small, and those lossy dips in the transmission spectrum are sharp.

As shown in Fig. 2(a), when we only filled the capillary with RIML, we could not distinguish the position of the resonant dip due to the large difference between the absolute values of the reflection coefficients r and r' on the inner and outer walls of the capillary. To improve the contrast of the fringe, UV adhesive is introduced to the outer surface of the capillary, so as to bring balance to the absolute values of r and r'. Before curing, the index value of the adhesive is 1.3685. In this case, the absolute value of r' is still smaller than that of r, and there is not much improvement in the spectrum, as seen in Fig. 2(b). However, with the increase of curing time, the refractive index of UV adhesive is increased to a higher value. The increase of the RI can be explained by the volume shrinkage of the UV-curing adhesive, which originates from the shortening of inter-atomic spacing [30]. As shown in Fig. 3, the main component of adhesive is acrylate. During polymerization, the chemical bond between acrylate monomer molecules changes from van der Waals force to co-valent bond, which leads to the closer distance between molecules [30]. The density of the adhesive increases as the molecules get closer, and leads to higher index value.

In order to investigate the effect of UV curing time on the transmission spectrum of the samples, the samples were cured for 60 min and the data were recorded every 10min interval. Fig. 4 shows the change of the transmission spectrum of the sample near 1400 nm band with the increase of UV curing time. It can be found from Fig. 4 that the resonant dip becomes more and more sharp within 20min of UV curing, but becomes gentle as the UV curing time continues to increase. This is because the refractive index of UV adhesive increases with the increase of curing time, and the refractive index is closest to 1.39 when curing for 20min. It is worth noting that from Fig. 4, we can find that the position of the resonant peak has shifted, which is because the ambient temperature of the sensor has

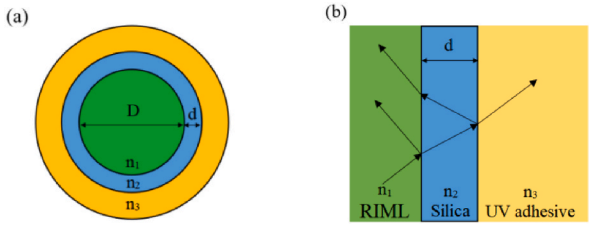

Fig. 5. (a): Schematic diagram of the cross-section of the modified waveguide. (b): Guiding mechanism of the hollow core fiber.

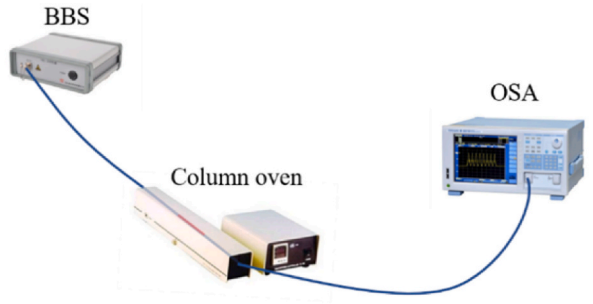

Fig. 6. Experimental setup for measuring the temperature by the proposed sensor.

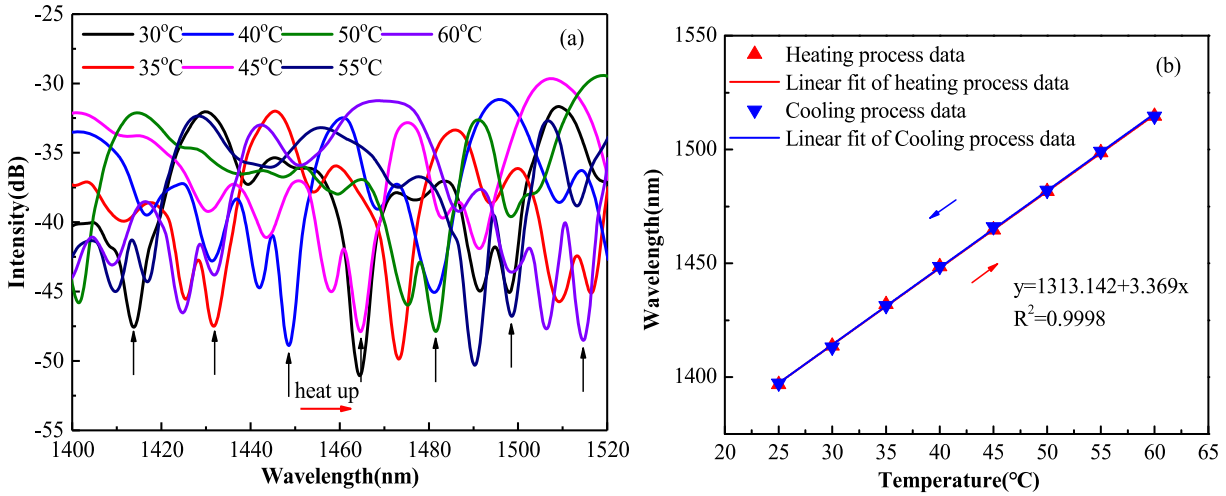

Fig. 7. (a): Measured transmission spectra of the sensor at different temperatures. (b): Wavelength response of the sensor at heating (red) and cooling (blue) processes. (For interpretation of the references to colour in this figure legend, the reader is referred to the Web version of this article.)

slightly increased under the ultraviolet lamp irradiation for a long time. For the above reasons, we controlled the UV curing time at 20min in order to obtain sharp resonant dip in the transmission spectrum. In this way, the resonant strength is strong in the silica cladding, and the fringe contrast is much better, as can be seen from Fig. 2(c).

Fig. 5(a) gives the cross section illustration of the modified waveguide, and Fig. 5(b) gives the optical path of the modified anti-resonant reflecting guidance. The location of the resonant wavelength can be given by,

$$\lambda = \frac{2d\sqrt{n_2^2 - n_1^2}}{m} \tag{2}$$

where n_1 and n_2 are the refractive indices of the RIML and silica, and m is the resonance order, respectively. The thickness of the ring cladding is 25 μm. By taking these values into Eq. (2), and also consider the influence of dispersion on the value od n_2, the resonant wavelength in the measurement range can be calculated to be at 1254 nm, 1324 nm, and 1402 nm. There is difference between the theoretical value and experimental value. This is because the values of n_1 and the thickness d might still not be so accurate compared with their real values, which causes the difference.

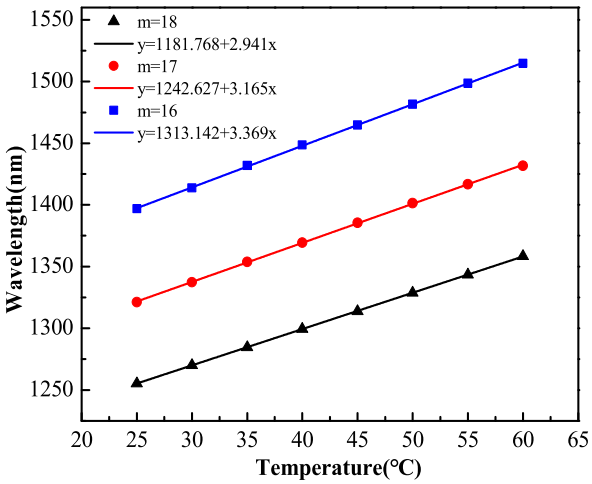

Fig. 8. Wavelength response of sensor with resonance orders of m = 16, 17 and 18.

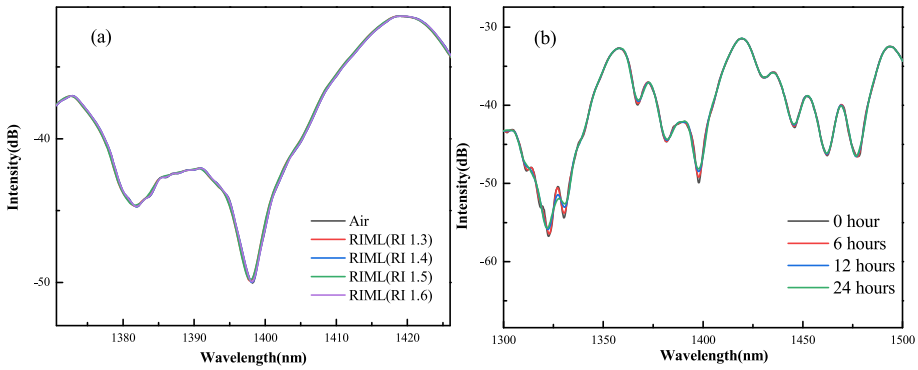

Fig. 9. (a):The transmission spectrum of the fabricated sensor in liquids of different index value. (b): Stability test of the sensor.

3. Sensing performance of the fiber sensor

Fig. 6 shows the temperature sensing set-up for our proposed sensor. Broadband source (BBS) and spectral analyzer (OSA) were used to monitor the output spectrum of the sensor. The sensor's thermal response is investigated by employing a heating and cooling treatment with a column oven (LCO 102). The manufactured sensor is put into the oven to monitor the transmission spectrum under different temperatures. The temperature is increased from room temperature to 60 °C, with a step of 5°. Each temperature is kept for 10 min for stabilization before recording the spectrum. Then the sensor is cooled down to room temperature in the same way as the heating process. Fig. 7(a) shows the transmission spectra of the sensor at different temperatures during the heating process.

The transmission dips are found to shift toward longer wavelength as temperature rises. The wavelength responses of the heating and cooling process are plotted in Fig. 7(b). The sensor exhibits a very linear response against temperature, and achieves a temperature sensitivity of 3.369 nm/°C. The temperature sensitivity of the sensor is given as,

$$\frac{d\lambda}{dT} = \frac{-2d(n_1C_1 - n_2C_2)}{m\sqrt{n_2^2 - n_1^2}} \tag{3}$$

where C_1 and C_2 are the thermo-optic coefficients of RIML and silica. The value of C_1 and C_2 are -3.44×10^{-4} and 1×10^{-5}, respectively. Equation (3) indicates that the temperature sensitivity is mainly affected by the thickness of the capillary(d), the index value of the infiltrated liquid (n_1) and the thermal-optic coefficient of the liquid, as well as the order of the resonance (m). The thermal response of different resonance orders is plotted in Fig. 8. The temperature sensitivities for m = 16, 17 and 18 are 3.369 nm/°C, 3.165 nm/°C and 2.941 nm/°C, respectively. The sensitivity decreases with resonance orders, which is in agreement with Eq. (3). The melting point of the adhesive restricts the measurement range of the sensor, however, compared with other sensor devices based on similar scheme (introduction of liquids), the measurement range of which is also small, our sensitivity relatively higher, and the structure is simple and cost effective.

The sensitivity of a sample does not fully quantify the performance of a sensor. The detection limit [28] represents the smallest

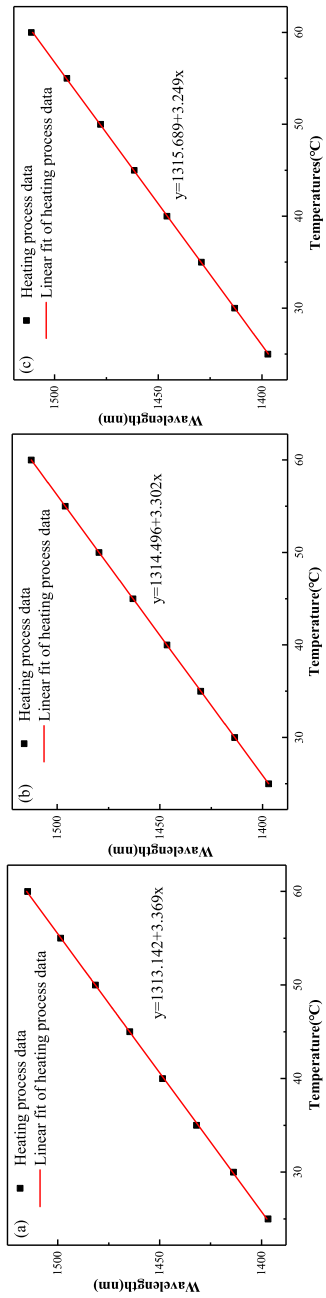

Fig. 10. (a)–(c):The repeatability test of temperature sensing.

amount of change that a sensor can detect, which is be defined as [31],

$$\delta T_L = \frac{\delta\lambda_0}{S} \tag{4}$$

For the monitored dip, the full width at half maximum (FWHM) is 3.59 nm. The resolution of the OSA is 0.02 nm. Assuming a signal-to-noise ratio of 50 dB, the detection limit is estimated to be 0.04 °C by Eq. (4).

In order to test whether the designed sensor is affected by the external environment, we put the prepared sensor in the refractive index matching liquids with the different index values (1.3, 1.4, 1.5 and 1.6), to observe the change of the transmission spectrum. As shown in Fig. 9(a), the change of external refractive index has little influence on the location of the resonant dip in the transmission spectrum. This is because the UV adhesive after curing isolate the waveguide from the surrounding wet environment. The stability of the sensor is also tested by recording the sensor spectrum in time scale of 24 h. Fig. 9(b) gives the spectrum at different time. The location of the transmission dips is quite stable during the test. The repeatability of the sensor is performed with three temperature tests on the same sample under the same measurement conditions, as shown in Fig. 10(a)~(c). The results show good repeatability of the temperature sensitivity with an average error of less than 3.6%.

4. Conclusions

In conclusion, we reported a highly sensitive temperature sensor based on modified anti-resonant reflecting guidance mechanism in silica capillary. The infiltration of liquids into the hollow core of the silica capillary alters the resonant condition of the waveguide, and causes the resonant wavelength to change. On the other hand, by coating the infiltrated capillary with UV cured adhesive, the reflectivities at both interfaces of the silica cladding is closer to each other, which enhances the resonant strength, and leads to improvement of the fringe visibility. The device is found to be exhibiting very high sensitivity against temperature. The transmission dips shift toward longer wavelength as temperature rises. Linear wavelength response is observed during the heating and cooling process, and a temperature sensitivity of 3.369 nm/°C is obtained from room temperature to 60 °C. The detection limit of the proposed sensor is 0.04 °C. The sensitivity is also found to be related to the resonant order. The proposed sensor is cost effective, easy to fabricate, with good reproducibility and high sensitivity, and is applicable in both dry and wet environments, which can be applicated in fields like biochemistry industry and pharmacy industry.

Author contribution statement

Wei Cheng: performed the experiments; wrote the paper.
Shuhui Liu: conceived and designed the experiments; analysis and interpreted the data.
Panting Niu: contributed reagents, materials, analysis tools or data; analyzed and interpreted the data.
Ting Chen: analyzed and interpreted the data.

Funding statement

Shuhui Liu was supported by National Natural Science Foundation of China [12004290; 51909195], Hubei Provincial Natural Science Foundation of China [2020CFB251], Scientific Research Project of Education Department of Hubei Province [Q20181501; Q20191512], State Key Laboratory of Advanced Optical Communication Systems and Networks [2020GZKF007], Headmaster Foundation of Wuhan Institute of Technology [2020133].

Data availability statement

Data will be made available on request.

Declaration of interest's statement

The authors declare no competing interests.

References

[1] Y. Lai, K. Zhou, K. Sugden, I. Bennion, Point-by-point inscription of first-order fiber Bragg grating for C-band applications, Opt Express 15 (2007), 18318.
[2] Y. Li, W. Chen, H. Wang, N. Liu, P. Lu, Bragg gratings in all-solid bragg photonic crystal fiber written with femtosecond pulses, J. Lightwave Technol. 29 (2011) 3367–3371.
[3] K.P. Koo, A.D. Kersey, Bragg grating-based laser sensors systems with interferometric interrogation and wavelength division multiplexing, J. Lightwave Technol. 13 (1995) 1243–1249.
[4] V. Bhatia, A.M. Vengsarkar, Optical fiber long-period grating sensors, Opt. Lett. 21 (1996) 692–694.
[5] G. Zhang, X. Wu, W. Zhang, S. Li, J. Shi, C. Zuo, S. Fang, B. Yu, High temperature vernier probe utilizing photonic crystal fiber–based Fabry–Perot interferometers, Opt Express 27 (2019), 37308.
[6] G. Zhang, X. Wu, S. Li, W. Liu, S. Fang, C. Zuo, W. Zhang, B. Yu, Miniaturized Fabry–Perot probe utilizing PMPCF for high temperature measurement, Appl. Opt. 59 (2020) 873.
[7] Q. Ge, J. Zhu, Y. Cui, G. Zhang, X. Wu, S. Li, H. Wang, B. Yu, Fiber optic temperature sensor utilizing thin PMF based Sagnac loop, Opt Commun. 502 (2022), 127417.

[8] I.S. Amiri, B.K. Paul, K. Ahmed, A.H. Aly, R. Zakaria, P. Yupapin, D. Vigneswaran, Tri-core photonic crystal fiber based refractive index dual sensor for salinity and temperature detection, Microw. Opt. Technol. Lett. 61 (2019) 847–852.
[9] M.S. Alam, S. Akter, B.K. Paul, K. Ahmed, D. Vigneswaran, M.N. Aktar, FEM based highly sensitive dual core temperature sensor: design and analysis, OSA Continuum 2 (2019) 2581–2592.
[10] M.A. Jabin, et al., Design and fabrication of amoeba faced photonic crystal fiber for biosensing application, Sensor Actuator Phys. 313 (2020), 112204.
[11] K. Ahmed, et al., Tetra-core surface plasmon resonance based biosensor for alcohol sensing, Phys. B Condens. Matter 570 (2019) 48–52.
[12] M. Jabin, et al., Titanium-coated dual-core D-shaped SPR-based PCF for hemoglobin sensing, Plasmonics 14.6 (2019) 1601–1610.
[13] A.A. Rifat, K. Ahmed, S. Asaduzzaman, B.K. Paul, R. Ahmed, Development of photonic crystal fiber-based gas/chemical sensors, Computational Photonic Sensors 12 (2019) 287–317.
[14] K. Ahmed, et al., Refractive index-based blood components sensing in terahertz spectrum, IEEE Sensor. J. 19.9 (2019) 3368–3375.
[15] H. Wang, M. Liao, H. Xiao, X. Han, Y. Jiang, J. Tan, P. Zhang, J. Shao, Y. Tian, J. Yang, High sensitivity temperature sensor based on a PDMS-assisted bow-shaped fiber structure, Opt Commun. 481 (2021), 126536.
[16] M.M. Hasan, H.J. Taher, S.A. Mohammed, Highly sensitive fiber-optic temperature sensor based on tapered no-core fiber for biomedical and biomechanical applications, PEN 9 (2021) 762.
[17] S. Wang, Y. Yang, P. Niu, S. Wu, S. Liu, R.-B. Jin, P. Lu, X. Hu, N. Dai, Fiber tip Michelson interferometer for temperature sensing based on polymer-filled suspended core fiber, Opt Laser. Technol. 141 (2021), 107147.
[18] J. Zhao, Y. Zhao, R.-Q. Lv, M.-Q. Chen, X.-G. Hu, Q. Zhao, A fiber ring cavity laser temperature sensor based on polymer-coated No-core fiber as tunable filter, IEEE Trans. Instrum. Meas. 70 (2021) 1–9.
[19] T. Han, Y. Liu, Z. Wang, J. Guo, Z. Wu, S. Wang, Z. Li, W. Zhou, Unique characteristics of a selective-filling photonic crystal fiber Sagnac interferometer and its application as high sensitivity sensor, Opt Express 21 (2013) 122–128.
[20] H. Liang, W. Zhang, P. Geng, Y. Liu, Z. Wang, J. Guo, S. Gao, S. Yan, Simultaneous measurement of temperature and force with high sensitivities based on filling different index liquids into photonic crystal fiber, Opt Express 38 (2013) 1071–1073.
[21] T. Han, Y. Liu, Z. Wang, Z. Wu, S. Wang, S. Li, Simultaneous temperature and force measurement using Fabry-Perot interferometer and bandgap effect of a fluid-filled photonic crystal fiber, Opt Express 20 (2012) 13320–13325.
[22] C. Zhao, Z. Wang, S. Zhang, L. Qi, C. Zhong, Z. Zhang, S. Jin, J. Guo, H. Wei, Phenomenon in an alcohol not full-filled temperature sensor based on an optical fiber Sagnac interferometer, Opt. Lett. 37 (2012) 4789–4791.
[23] M. Yang, D.N. Wang, Y. Wang, C. R Liao, Fiber in-line Mach–Zehnder interferometer constructed by selective infiltration of two air holes in photonic crystal fiber, Opt. Lett. 36 (2011) 636–638.
[24] W. Qian, C. Zhao, Y. Wang, C. Chan, S. Liu, W. Jin, Partially liquid-filled hollow-core photonic crystal fiber polarizer, Opt. Lett. 36 (2011) 3296–3298.
[25] Y. Peng, J. Hou, Y. Zhang, Z. Huang, R. Xiao, Q. Lu, Temperature sensing using the bandgap-like effect in a selectively liquid-filled photonic crystal fiber, Opt. Lett. 38 (2013) 263–265.
[26] S. Liu, M. Hou, J. Guo, Z. Li, P. Lu, Anti-resonant reflecting guidance in alcohol-filled hollow core photonic crystal fiber for sensing applications, Opt. Lett. 21 (2013) 31690–31697.
[27] P. Niu, S. Liu, W. Cheng, Liquid modified anti-resonant reflecting guidance in silica capillary for sensing applications, IEEE Access 10 (2022) 53676–53681.
[28] S. Liu, J. Tian, S. Wang, Z. Wang, P. Lu, Anti-resonant reflecting guidance in silica tube for high temperature sensing, IEEE Photon. Technol. Lett. 29 (2017) 2135–2138.
[29] S. Liu, J. Tian, N. Liu, J. Xia, P. Lu, Temperature insensitive liquid level sensor based on anti-resonant reflecting guidance in silica tube, J. Lighwave Technol. 34 (2016) 5239–5243.
[30] S. Liu, S. Cao, Z. Zhang, Y. Wang, C. Liao, Y. Wang, Temperature sensor based on side-polished fiber SPR device coated with polymer, Sensors 19 (2019) 4063.
[31] D.K.C. Wu, B.T. Kuhlmey, B.J. Eggleton, Ultrasensitive photonic crystal fiber refractive index sensor, Opt. Lett. 34 (2009) 322–324.